A Received Power Model for Reconfigurable Intelligent Surface and Measurement-based Validations

Zipeng Wang*, Li Tan*, Haifan Yin*, Kai Wang*, Xilong Pei*, David Gesbert†

*Huazhong University of Science and Technology, Wuhan, China

†EURECOM, Sophia-Antipolis, France

Email: wangzipeng0421@gmail.com, {ltan, yin, kaiw, pei}@hust.edu.cn, gesbert@eurecom.fr

Abstract—The idea of using a Reconfigurable Intelligent Surface (RIS) consisting of a large array of passive scattering elements to assist wireless communication systems has recently attracted much attention from academia and industry. A central issue with RIS is how much power they can effectively convey to the target radio nodes. Regarding this question, several power level models exist in the literature but few have been validated through experiments. In this paper, we propose a radar cross section-based received power model for an RIS-aided wireless communication system that is rooted in the physical properties of RIS. Our proposed model follows the intuition that the received power is related to the distances from the transmitter/receiver to the RIS, the angles in the TX-RIS-RX triangle, the effective area of each element, and the reflection coefficient of each element. To the best of our knowledge, this paper is the first to model the angle-dependent phase shift of the reflection coefficient, which is typically ignored in existing literature. We further measure the received power with our experimental platform in different scenarios to validate our model. The measurement results show that our model is appropriate both in near field and far field and can characterize the impact of angles well.

Index Terms—Reconfigurable intelligent surface, RIS, IRS, passive scattering elements, received power model, validations

I. INTRODUCTION

The fifth-generation (5G) wireless networks are under deployment over the world. As one of the key technologies in 5G, massive multiple-input-multiple-output (mMIMO) makes use of a large number of antennas (e.g., ≥ 64) to increase the spectral efficiency (SE) by, at least, an order of magnitude compared to 4G [1]. Despite this, both academia and industry continue their efforts to allow meeting ever more stringent requirements, such as ultra high data rate and energy efficiency, global coverage and connectivity, as well as extremely high reliability and low latency [2]. To solve these challenges, different avenues are considered, such as to further densify the network, using even ultra-massive MIMO arrays or utilizing the large and available bandwidth of higher frequency bands such as (sub-) terahertz frequencies [3] [4]. However, all these methods lead to higher energy consumption. Moreover, one of the major weaknesses for higher frequency bands is the limited network coverage, which is due to the high penetration loss and the lack of scattering and diffraction.

In parallel, a novel concept named reconfigurable intelligent surface has received more and more attention from academia

and industry [5]. It is also known as intelligent reflecting surfaces, large intelligent surfaces or software-controlled meta-surfaces. Briefly speaking, RIS is a two-dimensional (i.e., with near-zero thickness) surface consisting of a large array of passive scattering elements, each of which can be controlled in a software-defined manner to impose an amplitude change and/or phase shift to the incident signals. By tuning the reflecting phases of the incident signals independently, the reflected signals can be added coherently to improve the received signal power or combined destructively to mitigate interference when arriving at the user equipment (UE) [6]. In general, RIS is a prospective paradigm to realize a smart and reconfigurable wireless environment and improve the transmission performance with low energy consumption and hardware cost [7].

So far, numerous investigations have been performed on different aspects of RIS, such as prototyping [8] [9] [10], channel estimation [11] [12], promising application scenarios [13] [14], etc. Among them, the modeling of received power for RIS-aided wireless communication systems is a fundamental yet challenging work, which is of great significance to the understanding of the RIS technology itself. Although several received power models have been proposed, most of them are lacking in experimental validations. The authors of [15] make use of electromagnetic arguments to derive an exact channel gain expression that captures three essential near-field behaviors. [16] takes advantage of the physical optics techniques to derive the far-field pathloss model that is inversely proportional to the square of the product of distances. In [17], the received signal power is formulated as the sum of each scattering element's received power which is related to the distances between the RIS elements and the transceivers, the element gains, and the complex-valued coefficients of the elements. The authors in [18] develop a free-space pathloss model for RIS and experimental validations were also performed. Their proposed pathloss model is related to the distances from transceivers to the RIS, the size of the RIS, and the radiation patterns of antennas and elements.

In this paper, we propose a novel radar cross section (RCS)-based received power model. To the best of our knowledge, our model is the first that takes angles of incidence/reflection into account when describing the phase shifts of the reflection

elements. More specifically, the reflection phase in our model is not only a function of the control voltage imposed on the RIS element, but also a function of the angles. This is an important fact to consider when calculating the desired reflection coefficients. We validate the proposed model on our hardware platform and show that the simulation results based on our proposed model are very close to measurements.

II. SYSTEM MODEL

We consider an RIS-aided wireless communication system as shown in Fig. 1. For simplicity, the transmitter and receiver are both equipped with a single antenna. However, the results of this paper can be easily generalized to the case of MIMO.

Since the model of line of sight (LOS) propagation between the transmitter and the receiver is well known, we focus on modeling the signals reflected by the RIS in this paper only. In case the LOS path exists, we just need to add the signal of the LOS path and the reflected paths. Referring to Fig. 1, the RIS with $M \times N$ elements is placed on the x-y plane of a Cartesian coordinate system and each row is parallel to the x-axis. The origin of the coordinate system is located at the geometric center of the RIS. Let $E_{m,n}$ denote the element in the m-th row and n-th column. The length and width of an element are denoted by dx and dy, respectively. The location of $E_{m,n}$ is expressed as

$$\boldsymbol{p}_{m,n} = \left(\left(n - \frac{N+1}{2} \right) dx, \left(\frac{M+1}{2} - m \right) dy, 0 \right) \quad (1)$$

in the Cartesian coordinate system.

Furthermore, we use the spherical coordinates to represent the positions of the transmitter/receiver. Specifically, $(d_1, \theta_1, \varphi_1)$ and $(d_2, \theta_2, \varphi_2)$ denote the positions of the transmitter and receiver seen from the geometric center of the RIS plane, where d, θ, φ represent the equivalent distance, zenith angle and azimuth angle, respectively. If seen from $E_{m,n}$, the positions of the transmitter and receiver can be expressed as $\left(d_{m,n}^t, \theta_{m,n}^t, \varphi_{m,n}^t \right)$ and $\left(d_{m,n}^r, \theta_{m,n}^r, \varphi_{m,n}^r \right)$. The spherical coordinates can be transformed into Cartesian coordinates by

$$\begin{cases} C_x = d \sin\theta \cos\varphi, \\ C_y = d \sin\theta \sin\varphi, \\ C_z = d \cos\theta. \end{cases} \quad (2)$$

Denote the transmit signal as x. The received signal is written as

$$y = \left(\sum_{m=1}^{M} \sum_{n=1}^{N} h_{m,n} g_{m,n} \Gamma_{m,n} \right) x + z, \quad (3)$$

where $h_{m,n}$ is the channel coefficient between the transmitter and the reflecting element $E_{m,n}$, and $g_{m,n}$ is the channel coefficient between $E_{m,n}$ and the receiver. z is the noise. $\Gamma_{m,n}$ is the reflection coefficient of the element $E_{m,n}$.

III. THE RECEIVED POWER MODEL

In this section, we propose a general model for the received power in the RIS-aided communication system. Denote the transmit power by P_t and transmit antenna gain by $G_t \left(\mathbf{r}_{m,n}^t \right)$,
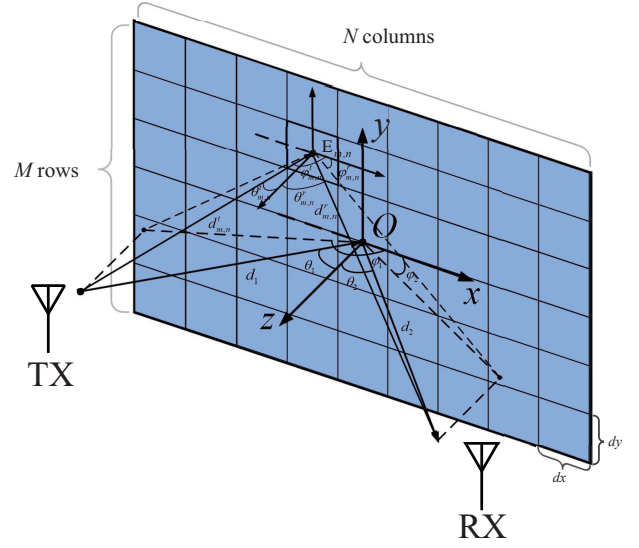

Fig. 1. The geometric illustration of an RIS-aided communication system.

where $\mathbf{r}_{m,n}^t$ represents the direction from the transmitter to the element $E_{m,n}$ and is related to $\theta_{m,n}^t$ and $\varphi_{m,n}^t$. Then the spatial power density generated by the transmitter on the element $E_{m,n}$ is

$$S_{m,n}^t = P_t G_t \left(\mathbf{r}_{m,n}^t \right) \frac{1}{4\pi \left(d_{m,n}^t \right)^2}, \quad (4)$$

where $d_{m,n}^t$ represents the distance from the transmitter to $E_{m,n}$. With the transmitter located at (C_x, C_y, C_z), $d_{m,n}^t$ can be calculated by

$$d_{m,n}^t = \sqrt{\left[C_x - \left(n - \frac{N+1}{2} \right) dx \right]^2 + \left[C_y - \left(\frac{M+1}{2} - m \right) dy \right]^2 + C_z^2}. \quad (5)$$

The power captured by $E_{m,n}$ is

$$P_{m,n}^t = S_{m,n}^t A_e \left(-\mathbf{r}_{m,n}^t \right), \quad (6)$$

where $A_e \left(-\mathbf{r}_{m,n}^t \right)$ is the effective area of the m, n-th element in the direction $-\mathbf{r}_{m,n}^t$. Similar to (4), the spatial power density generated by the m, n-th element is

$$S_{m,n}^r = P_{m,n}^t G_e \left(\mathbf{r}_{m,n}^r \right) \frac{1}{4\pi \left(d_{m,n}^r \right)^2}, \quad (7)$$

where $d_{m,n}^r$ represents the distance from $E_{m,n}$ to the receiver, which can be calculated similarly to (5). $G_e \left(\mathbf{r}_{m,n}^r \right)$ is the gain of the element $E_{m,n}$ in the direction $\mathbf{r}_{m,n}^r$. The relation between the effective area and element gain is generally expressed as [19]

$$G_e \left(\mathbf{r}_{m,n}^r \right) = \frac{4\pi}{\lambda^2} A_e \left(\mathbf{r}_{m,n}^r \right). \quad (8)$$

Note that we do not consider the power loss of the reflection in (8). However, the efficiency of the reflection will later be taken into account in the reflection coefficient. The power captured by the receiver from the m, n-th element is

$$P_{m,n}^r = S_{m,n}^r A_r \left(-\mathbf{r}_{m,n}^r \right), \quad (9)$$

where $A_r\left(-\mathbf{r}^r_{m,n}\right)$ is the effective area of the receiving antenna in the direction $-\mathbf{r}^r_{m,n}$, which has the similar relation with antenna gain $G_r\left(-\mathbf{r}^r_{m,n}\right)$, namely

$$A_r\left(-\mathbf{r}^r_{m,n}\right) = \frac{\lambda^2}{4\pi\eta_r}G_r\left(-\mathbf{r}^r_{m,n}\right), \quad (10)$$

where $\eta_r \in [0,1]$ is the efficiency of the receiving antenna. According to (4) $\sim$ (10), the received power reflected from the m, n-th element is

$$P^r_{m,n} = P_t G_t\left(\mathbf{r}^t_{m,n}\right) G_r\left(-\mathbf{r}^r_{m,n}\right) \frac{A_e\left(-\mathbf{r}^t_{m,n}\right) A_e\left(\mathbf{r}^r_{m,n}\right)}{\left(4\pi d^t_{m,n}d^r_{m,n}\right)^2 \eta_r}. \quad (11)$$

Some recent experiments in [10] have indicated that both the amplitude and phase shift of the reflection coefficient are related to the angle of incidence, the angle of reflection, and the control signal, e.g., the bias voltage of a varactor. An example is that, for a given control signal, the reflection coefficient also varies with the angles of arrival and departure. As a result, we model the reflection coefficient as a function of the three factors mentioned above. For the element $\mathrm{E}_{m,n}$, the reflection coefficient is modeled as

$$\Gamma_{m,n}\left(-\mathbf{r}^t_{m,n}, \mathbf{r}^r_{m,n}, u_{m,n}\right) \quad (12)$$
$$= \mu_{m,n}\left(-\mathbf{r}^t_{m,n}, \mathbf{r}^r_{m,n}, u_{m,n}\right) \mathrm{e}^{\mathrm{j}\phi_{m,n}\left(-\mathbf{r}^t_{m,n}, \mathbf{r}^r_{m,n}, u_{m,n}\right)},$$

where $\mu_{m,n}\left(-\mathbf{r}^t_{m,n}, \mathbf{r}^r_{m,n}, u_{m,n}\right)$, $\phi_{m,n}\left(-\mathbf{r}^t_{m,n}, \mathbf{r}^r_{m,n}, u_{m,n}\right)$ represent the amplitude attenuation and phase shift, respectively. $u_{m,n}$ is the control signal imposed on the element $\mathrm{E}_{m,n}$.

The total received power reflected by the RIS is then written as

$$P_r = \left|\sum_{m=1}^{M}\sum_{n=1}^{N}\Gamma_{m,n}\left(-\mathbf{r}^t_{m,n}, \mathbf{r}^r_{m,n}, u_{m,n}\right)\sqrt{P^r_{m,n}}\mathrm{e}^{\mathrm{j}\Phi_{m,n}}\right|^2, \quad (13)$$

where $\Phi_{m,n}$ is the phase difference of the m, n-th element caused by the propagation delay:

$$\Phi_{m,n} = \frac{2\pi}{\lambda}\left(d^t_{m,n} + d^r_{m,n}\right). \quad (14)$$

In order to make the expression more intuitive, the concept of radar cross section (RCS) $\sigma_{m,n}\left(-\mathbf{r}^t_{m,n}, \mathbf{r}^r_{m,n}, u_{m,n}\right)$ is introduced to describe the joint impact of the amplitude attenuation and the effective area of the element $\mathrm{E}_{m,n}$, namely

$$\sigma_{m,n}\left(-\mathbf{r}^t_{m,n}, \mathbf{r}^r_{m,n}, u_{m,n}\right) \quad (15)$$
$$= \mu_{m,n}\left(-\mathbf{r}^t_{m,n}, \mathbf{r}^r_{m,n}, u_{m,n}\right)\sqrt{A_e\left(-\mathbf{r}^t_{m,n}\right) A_e\left(\mathbf{r}^r_{m,n}\right)}.$$

The proposed received power model can now be written as

$$P_r = \frac{P_t}{16\pi^2\eta_r}\left|\sum_{m=1}^{M}\sum_{n=1}^{N}\frac{\sqrt{G_t G_r}\sigma_{m,n}\mathrm{e}^{\mathrm{j}(\phi_{m,n}+\Phi_{m,n})}}{d^t_{m,n}d^r_{m,n}}\right|^2. \quad (16)$$

Note that we temporarily drop the arguments of G_t, G_r, $\sigma_{m,n}$ and $\Phi_{m,n}$ in order to make the above expression more concise.

We now study the impact of angles on the RCS, which depends on multiple parameters, e.g., the incident/reflection angles and the efficiency of reflection. In practice, such a multi-dimensional data can be obtained by electromagnetic simulate software. For simplicity however, we let the angles of θ^t and φ^t both equal to zero degree(also the case in our experiments), and characterize the impact of zenith angle of reflection θ^r on the RCS $\hat{\sigma}$. we adopt the model of [20] here:

$$\hat{\sigma}\left(\theta^r\right) = \frac{4\pi A^2}{\lambda^2}\left[\frac{\sin\left(k\sqrt{A}\sin\left(\theta^r\right)\right)}{k\sqrt{A}\sin\left(\theta^r\right)}\right]^2 + c, \quad (17)$$

where $A = dxdy$ is the geometry area of each element and $k = \frac{2\pi}{\lambda}$ is the wave number. c is a constant which is related to other parameters, e.g., the reflection efficiency and/or the angle φ^r.

We now characterize the impact of θ^r on the phase shift. We propose to model such a relationship with a cosine function:

$$\hat{\phi}\left(\theta^r\right) = a\cos\left(\theta^r\right) + b, \quad (18)$$

where a, b are the design parameters. An example of their values is given below.

Fig. 2 illustrates the reflection coefficient as a function of θ^r with azimuth angle φ^r fixed to $45°$. We can observe that our models fit the CST simulations well.
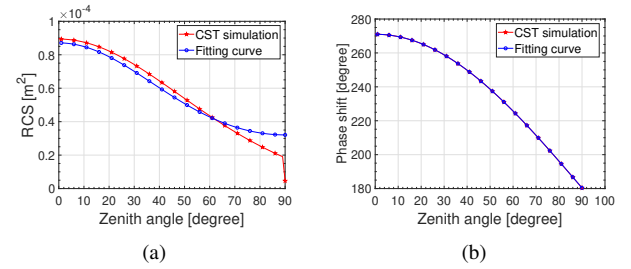

Fig. 2. The reflection coefficient versus the zenith angle θ^r with $\phi = 45°$. (a) $\hat{\sigma}$ versus θ^r with $c = 1.42\times10^{-5}$ m^2. (b) $\hat{\phi}$ versus θ^r with $a = 90°, b = 180°$.

IV. MEASUREMENTS AND VALIDATIONS

In this section, we validate the proposed model with measurements and compare it with an existing model. Some recent works have modeled the role of RIS as the specular reflection approximately when in the near field (i.e., $d_1, d_2 \leq d_f$, where d_f is the boundary of near field and far field) or the RIS is infinitely large (i.e., $Mdy, Ndx \geq 10\lambda$) [18]. It means that the RIS acts as a plane mirror that reflects the incident signal with the same amplitude attenuation coefficient and perfect phase shift. Similar to the Friis transmission equation, the received power of the specular reflection model is expressed as

$$P_r = P_t G_t G_r\left[\frac{\lambda\bar{\mu}}{4\pi\left(d_1 + d_2\right)}\right]^2, \quad (19)$$

where $\bar{\mu}$ is the average amplitude of the reflection coefficient

$$\bar{\mu} = \frac{1}{MN}\sum_{m=1}^{M}\sum_{n=1}^{N}\mu_{m,n}\left(-\mathbf{r}^t_{m,n}, \mathbf{r}^r_{m,n}, u_{m,n}\right), \quad (20)$$

and G_t, G_r are the antenna gains.

From (19), one may observe that the received signal power is inversely proportional to $(d_1 + d_2)^2$. In the following we will validate this model and our proposed model (16).

Fig. 3 illustrates the indoor and outdoor measurement environments. The reflection coefficients are 1-bit quantized, i.e., the two control states have a phase difference of around 180 degrees, which is enabled by adjusting the bias voltage $u_{m,n}$ imposed to the varactor diodes. The basic parameters of our experiments are listed in Table I. Other details of our experimental platform can be found in [10].

TABLE I
BASIC PARAMETERS OF THE EXPERIMENTS

Parameters	Value
Operating frequency	$f = 5.8$ GHz
Antenna peak gain	$G_t = G_r = 17.1$ dB
Efficiency of antenna	$\eta_r \approx 54.29\%$
Rows and columns	$M = 20, N = 55$
Element size	$dx = 14.3$ mm, $dy = 10.27$ mm

We carry on near-field experiments indoor and far-field experiments outdoor. The boundary of near field and far field is defined as [18]

$$d_f = \frac{2MN dx dy}{\lambda^2}. \tag{21}$$

For the RIS in our tests, the boundary $d_f \approx 6$ m. Thus, we select the distances from 1 m to 5 m in indoor near-field experiments and from 5 m to 50 m in outdoor far-field experiments. The antennas are placed in a way that the azimuth angles of the transmit/receive antennas seen from the origin of the RIS are always equal to zero degree(i.e., $\varphi_1 = \varphi_2 = 0$).

Fig. 4 illustrates the indoor near-field measurement results and the model results of the power attenuation P_r/P_t as a function of the distance between the transmitter and the geometric center of the RIS (i.e., d_1). We can observe that the measurements have the same trend with our proposed RX power model, however with a gap of about 2 dB. This difference might be due to the reflection of indoor metal objects and walls. When it comes to the curve of the specular reflection model, it is also close to the measurement results in such a near-field case. These measurements validate the applicability of the received power model we proposed and the specular reflection model in this case.

Fig. 5 illustrates the outdoor far-field results of the power attenuation. We can observe that there is an increasing gap between the specular reflection model and the measurement results. However, simulation results based on our model are consistent with the measurements, which validates the accuracy of the proposed received power model in far-field case.

Fig. 6 illustrates the indoor power attenuation results as a function of the zenith angle of the receiver (i.e., θ_2). We observe that the RX received power model we proposed matches the measurements with a gap of about 2 dB. Since the specular reflection model does not consider the influence of angles, the received power model is a constant value, which is not aligned with the measured results.
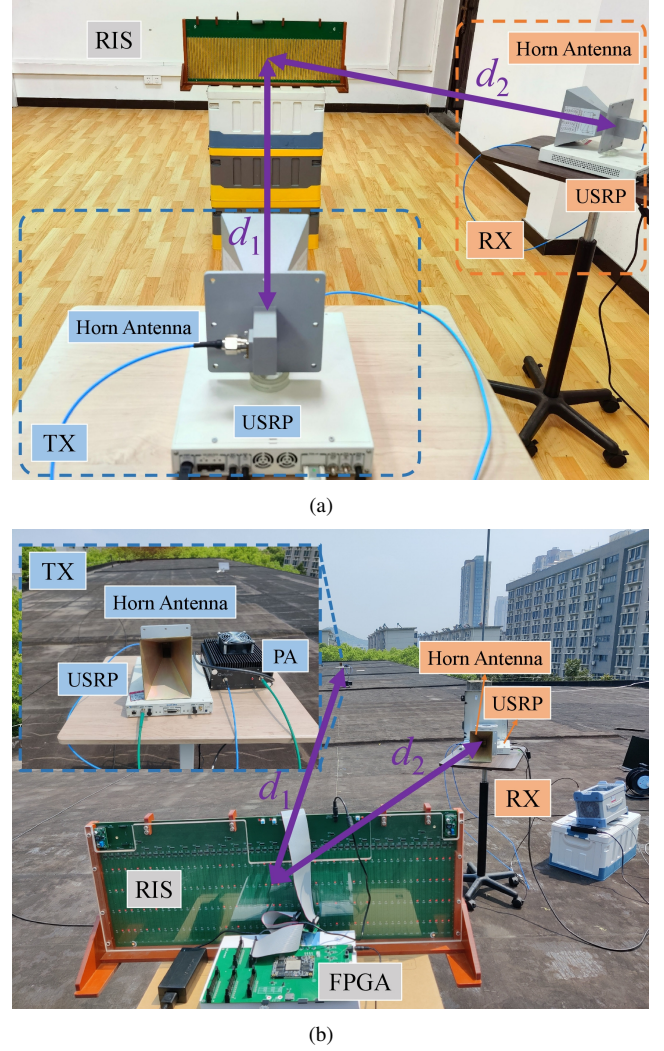

Fig. 3. Measurement environments. (a) Indoor near field testing scene. (b) Outdoor far field testing scene.
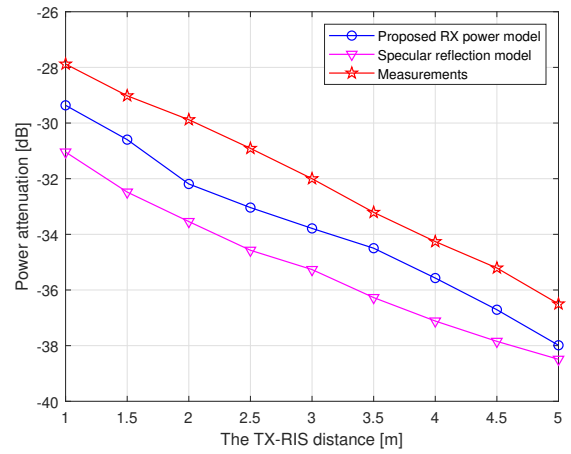

Fig. 4. Power attenuation versus the TX-RIS distance d_1 with $d_2 = 2, \theta_1 = 0, \theta_2 = 30°, \varphi_1 = 0, \varphi_2 = 0$.
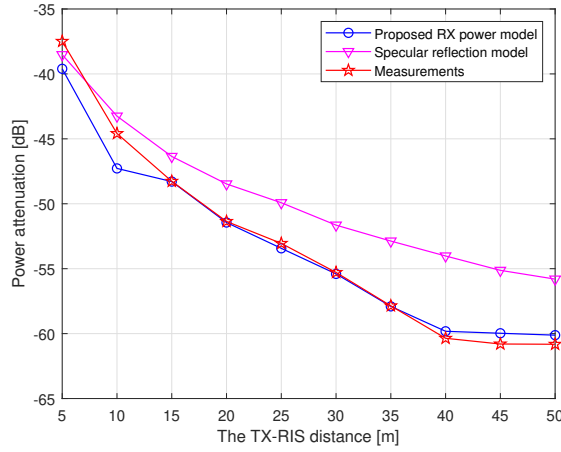
Fig. 5. Power attenuation versus the TX-RIS distance d_1 with $d_2 = 2, \theta_1 = 0, \theta_2 = 30°, \varphi_1 = 0, \varphi_2 = 0$.
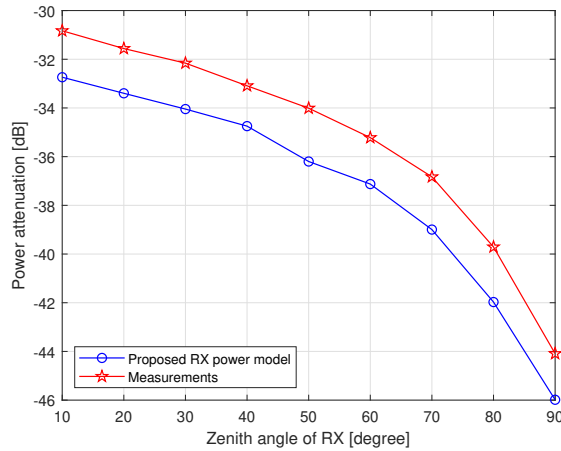

Fig. 6. Power attenuation versus the zenith angle of RX θ_2 with $d_1 = 3, d_2 = 2, \theta_1 = 0, \varphi_1 = 0, \varphi_2 = 0$.

V. Conclusion

In this work, we have proposed a novel RCS-based received power model for an RIS-aided wireless communication system. This model introduces an angular-dependent phase shift behavior of the RIS elements, which has not yet been considered in previous models. We then validated it through indoor and outdoor measurements. The results show that the specular reflection model is able to describe the received power in near-field case when the incident/reflection angles are relatively small. However it fails when in the far-field case or in case the angles are large. By contrast, our model can hold for both near-field and far-field cases and it can characterize the impact of the angles well.

Acknowledgment

References

[1] T. L. Marzetta, "Noncooperative cellular wireless with unlimited numbers of base station antennas," *IEEE Trans. Wireless Commun.*, vol. 9, no. 11, pp. 3590–3600, Nov. 2010.

[2] W. Saad, M. Bennis, and M. Chen, "A vision of 6G wireless systems: Applications, trends, technologies, and open research problems," *IEEE Network*, vol. 34, no. 3, pp. 134–142, 2020.

[3] F. Boccardi, R. W. Heath, A. Lozano, T. L. Marzetta, and P. Popovski, "Five disruptive technology directions for 5G," *IEEE Commun. Mag.*, vol. 52, no. 2, pp. 74–80, 2014.

[4] N. Rajatheva, I. Atzeni, E. Bjornson, A. Bourdoux, and W. Xu, "White Paper on Broadband Connectivity in 6G," *arXiv e-prints*, p. arXiv:2004.14247, Apr. 2020.

[5] Q. Wu and R. Zhang, "Towards smart and reconfigurable environment: Intelligent reflecting surface aided wireless network," *IEEE Commun. Mag.*, vol. 58, no. 1, pp. 106–112, 2020.

[6] S. Gong, X. Lu, D. T. Hoang, D. Niyato, L. Shu, D. I. Kim, and Y. C. Liang, "Towards smart wireless communications via intelligent reflecting surfaces: A contemporary survey," *IEEE Commun. Surv. Tutor.*, vol. 22, no. 4, pp. 2283–2314, Fourthquarter 2020.

[7] C. Huang, A. Zappone, G. C. Alexandropoulos, M. Debbah, and C. Yuen, "Reconfigurable intelligent surfaces for energy efficiency in wireless communication," *IEEE Trans. Wireless Commun.*, vol. 18, no. 8, pp. 4157–4170, 2019.

[8] W. Tang, X. Li, J. Y. Dai, S. Jin, Y. Zeng, Q. Cheng, and T. J. Cui, "Wireless communications with programmable metasurface: Transceiver design and experimental results," *China Commun.*, 2019.

[9] L. Dai, B. Wang, M. Wang, X. Yang, J. Tan, S. Bi, S. Xu, F. Yang, Z. Chen, M. D. Renzo, C.-B. Chae, and L. Hanzo, "Reconfigurable intelligent surface-based wireless communications: Antenna design, prototyping, and experimental results," *IEEE Access*, vol. 8, pp. 45 913–45 923, 2020.

[10] X. Pei, H. Yin, L. Tan, L. Cao, Z. Li, K. Wang, K. Zhang, and E. Björnson, "RIS-Aided Wireless Communications: Prototyping, Adaptive Beamforming, and Indoor/Outdoor Field Trials," *arXiv e-prints*, p. arXiv:2103.00534, Feb. 2021.

[11] B. Zheng and R. Zhang, "Intelligent reflecting surface-enhanced OFDM: Channel estimation and reflection optimization," *IEEE Wireless Commun. Lett.*, vol. 9, no. 4, pp. 518–522, 2020.

[12] L. Wei, C. Huang, G. C. Alexandropoulos, C. Yuen, Z. Zhang, and M. Debbah, "Channel estimation for ris-empowered multi-user miso wireless communications," *IEEE Trans. Commun.*, vol. 69, no. 6, pp. 4144–4157, 2021.

[13] Y.-C. Liang, R. Long, Q. Zhang, J. Chen, H. V. Cheng, and H. Guo, "Large intelligent surface/antennas (LISA): Making reflective radios smart," *J. Commun. Netw.*, vol. 4, no. 2, pp. 40–50, 2019.

[14] M. Di Renzo, A. Zappone, M. Debbah, M.-S. Alouini, C. Yuen, J. de Rosny, and S. Tretyakov, "Smart radio environments empowered by reconfigurable intelligent surfaces: How it works, state of research, and the road ahead," *IEEE J. Sel. Areas Commun.*, vol. 38, no. 11, pp. 2450–2525, 2020.

[15] E. Björnson and L. Sanguinetti, "Power scaling laws and near-field behaviors of massive MIMO and intelligent reflecting surfaces," *IEEE Open J. Commu. Soc.*, vol. 1, pp. 1306–1324, 2020.

[16] Özdogan Özgecan, E. Björnson, and E. G. Larsson, "Intelligent reflecting surfaces: Physics, propagation, and pathloss modeling," *IEEE Wireless Commun. Lett.*, vol. 9, no. 5, pp. 581–585, 2020.

[17] S. W. Ellingson, "Path Loss in Reconfigurable Intelligent Surface-Enabled Channels," *arXiv e-prints*, p. arXiv:1912.06759, Dec. 2019.

[18] W. Tang, M. Z. Chen, X. Chen, J. Y. Dai, Y. Han, M. Di Renzo, Y. Zeng, S. Jin, Q. Cheng, and T. J. Cui, "Wireless communications with reconfigurable intelligent surface: Path loss modeling and experimental measurement," *IEEE Trans. Wireless Commun.*, vol. 20, no. 1, pp. 421–439, Jan. 2021.

[19] M. Gustafsson and M. Capek, "Maximum gain, effective area, and directivity," *IEEE Trans Antennas Propag.*, vol. 67, no. 8, pp. 5282–5293, 2019.

[20] N. Levanon, "Radar," in *Encyclopedia of Physical Science and Technology (Third Edition)*, 3rd ed., R. A. Meyers, Ed. New York: Academic Press, 2003, pp. 497–510.